ChemBioChem

Research Article
doi.org/10.1002/cbic.202200570

Chemistry Europe
European Chemical Societies Publishing

www.chembiochem.org

Amber Light Control of Peptide Secondary Structure by a Perfluoroaromatic Azobenzene Photoswitch

Eleonora Cataldi[+],[a] Martina Raschig[+],[a] Marcus Gutmann,[a] Patrick T. Geppert,[c] Matthias Ruopp,[a] Marvin Schock,[a] Hubert Gerwe,[a] Rüdiger Bertermann,[c] Lorenz Meinel,[a, b] Maik Finze,[c] Agnieszka Nowak-Król,[c] Michael Decker,[a] and Tessa Lühmann*[a]

The incorporation of photoswitches into the molecular structure of peptides and proteins enables their dynamic photocontrol in complex biological systems. Here, a perfluorinated azobenzene derivative triggered by amber light was site-specifically conjugated to cysteines in a helical peptide by perfluoroarylation chemistry. In response to the photoisomerization (*trans*→*cis*) of the conjugated azobenzene with amber light, the secondary structure of the peptide was modulated from a disorganized into an amphiphilic helical structure.

Introduction

Photoswitches can modulate molecular geometry in response to light, enabling the design of light-controllable (bio)molecules.[1] Azobenzene derivatives respond to the energy of light illumination with *trans*↔*cis* isomerization. Previous studies of the unmodified azobenzene backbone showed that, due to the change in the geometry of the *cis* isomer, which is evidenced by the change in the spacing of the carbon atoms in the 4,4′ positions, the dipole moment is increased from 0 to 3 D, whereas intermolecular interactions, including van der Waals interactions, π–π stacking and lattice energy are weakened.[2] Thus, altered steric molecular structure leads to changes in the geometrical and thus physical properties of photoswitches. However, *cis* isomers spontaneously revert in the dark or via visible light-assisted processes into *trans* isomers, which are more stable in agreement with their lower free enthalpy.[3]

Azobenzenes have been successfully employed to photocontrol biomacromolecule functions, pharmaceutical ligands, biopolymers and materials including lipids, gold nanoparticles and ionic crystals.[1a,4] Their response to light and rate of reaching thermal equilibrium are related to the electronic and steric nature of the azobenzene core. Chemical substitutions on azobenzene aromatic rings tune the absorption spectra.[4f,5] Accordingly, structural modification of azobenzene derivatives can produce compounds with the absorption spectra bathochromically shifted to the red spectral ranges. These photoswitches are responsive to light, which penetrates tissues better than the light of lower wavelengths, which could in the future allow isomerization in deeper tissue layers, reduce scattering, and have safety advantages as compared to the use of ultraviolet light (UV).[4m]

Previous studies detailed the optical properties of azobenzene derivatives as photoswitches responsive to long wavelengths and their ability to photocontrol the secondary structure of peptides and proteins.[6] Woolley's group has extensively described the strategic introduction of electron-donating groups (EDGs), such as alkoxy (–OR) and thioether (–SEt), at the *ortho*- or asymmetrical *ortho*- and *meta*-azobenzene positions. This increased sensitivity to red light irradiation (>600 nm).[4j,n,p–r,7] They successfully incorporated a tetra-*ortho*-alkoxy substituted azobenzene in EAAAR-based peptides, controlling the peptide helical content through irradiation at $\lambda > 600$ nm, and having an increased half-life of hours/days. The limitation was found on its instability in reducing environment, which was addressed by a tetra-*ortho* chloride azobenzene derivative but with less efficiency on photoisomerization.[4q] Moreover, *ortho*-fluoroazobenzene-based photoswitches showed effective isomerization with visible light and long thermal half-lives.[4t,8] Fluorinated azobenzenes functionalized with a piperazine-2,5-dione derivative successfully controlled self-assemblies of a cyclic dipeptide.[9] Modified azobenzenes can also be used to control the α-helix conformation of cell-penetrating peptides (CPPs).[10]

CPPs (<30 amino acids long) might facilitate cellular uptake of drugs, including proteins and oligonucleotides (siRNA, DNA,

[a] E. Cataldi,[+] M. Raschig,[+] Dr. M. Gutmann, M. Ruopp, M. Schock, H. Gerwe, Prof. Dr. Dr. L. Meinel, Prof. Dr. M. Decker, Prof. Dr. T. Lühmann
Universität Würzburg, Institute for Pharmacy and Food Chemistry
Am Hubland, 97074 Würzburg (Germany)
E-mail: tessa.luehmann@uni-wuerzburg.de
[b] Prof. Dr. Dr. L. Meinel
Helmholtz Institute for RNA-Based Infection Research (HIRI)
Helmholtz Center for Infection Research (HZI)
97080 Würzburg (Germany)
[c] P. T. Geppert, Dr. R. Bertermann, Prof. Dr. M. Finze, Prof. Dr. A. Nowak-Król
Universität Würzburg, Institute of Inorganic Chemistry and
Institute for Sustainable Chemistry and Catalysis with Boron
Am Hubland, 97074 Würzburg (Germany)
[+] These authors contributed equally to this work.

Supporting information for this article is available on the WWW under https://doi.org/10.1002/cbic.202200570

etc.), small molecules and nanoparticles.[11] Leucine-lysine (LK) peptides, mainly containing basic lysine and nonpolar leucine residues, belong to the α-helical secondary amphipathic class of CPPs. The amino acid orientation through the helix forms two faces: hydrophobic and hydrophilic.[10,12] Stabilization of the α-helix conformation is essential for transmembrane transport. These LK CPPs were previously modified with an azobenzene external brace to control LK secondary structure by UV light.[10] Compared to other methods for stapled peptides, the use of azobenzenes has the advantage that a reversible stabilization of the helix and thus, a control of the cellular uptake can be achieved.[10,13]

In this work, we report the synthesis and photochemical properties of a perfluorinated azobenzene derivative and modification of a synthetic CPP deploying perfluoroarylation chemistry. We aimed to control the helical content of long-lived *cis*-azobenzenes through amber-light triggering for an efficient *ex vivo* ON/OFF switch. The nucleophilic aromatic substitution (S_NAr) reaction between the perfluoroaromatic azobenzene photoswitch and model thiolates was chemoselective and regiospecific. Moreover, it could be carried out under mild conditions affording the target compounds in high yields. Finally, we conjugated the perfluorinated azobenzene to an amphiphilic helical peptide and proved successful *trans*↔*cis* isomerization after irradiation with amber light.

Results and Discussion

Synthesis and performance of a perfluoroaromatic azobenzene photoswitch

Decafluoroazobenzene (DFAB) was synthesized by symmetrical oxidative homocoupling of pentafluoroaniline in an overall yield of 40%. Product identity was confirmed by ^{19}F NMR and purity by HPLC (Figure 1A and Figures S1, S4A, C in the Supporting Information).

Trans-DFAB in ACN showed two absorption bands, one at $\lambda_{max} = 305$ nm and a weaker one at $\lambda_{max} = 455$ nm, corresponding to the π–π* and n–π* electronic transitions, respectively (Figure 1B, C).[8c] We further tested the optical properties of the perfluorinated azobenzene photoswitch in response to light of

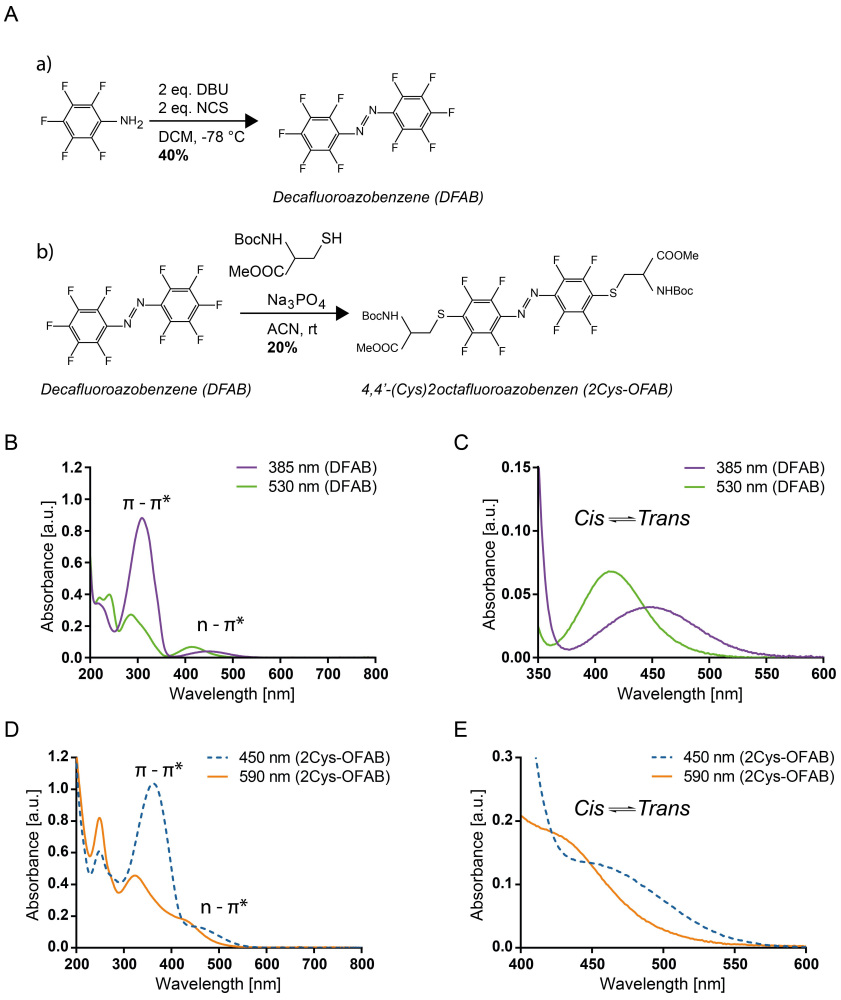

Figure 1. A) Synthesis of a) DFAB and b) 2Cys-OFAB. B) UV-Vis spectra overview and C) zoom of DFAB. D) UV-Vis spectra overview and E) zoom of 2Cys-OFAB. Electronic transition between the two isomers after irradiation: n–π* and π–π*.

various wavelengths ranging from 365 to 590 nm (15 minutes' irradiation; Figure S5A). Upon its irradiation at 530 nm (green light) the photostationary state $PSS_{530\,nm}$ was reached with the thermodynamically less stable *cis* isomer as the main species. The increase of the *cis* isomer concentration was accompanied by a reduction of the intensity of the π–π* absorption band at 305 nm (*trans* isomer) and an increase in intensity of the blue-shifted n–π* band at 415 nm (*cis* isomer). The n–π* band separation of 2170 cm^{-1} (40 nm) between the two isomers increased the n–π* bidirectional conversion rate with two different wavelengths *cis*→*trans*$_{385\,nm}$ and *trans*→*cis*$_{530\,nm}$ (Figure 1C).

To gain further insight into the *cis*→*trans* and *trans*→*cis* photoisomerization process, we performed *in-situ* illumination NMR experiments. To this end, we used an optical fiber-based NMR illumination setup, reported by Gschwind, which allows the monitoring of the processes in real time through irradiation of the DFAB samples followed by the instantaneous acquisition of ^{19}F NMR spectra.[14] The molar fractions of *cis* and *trans* isomers are derived from the ratio of the integrals of all fluorine signals corresponding to the *cis* and *trans* isomers (see the assignment of the signals and their chemical shifts in the Experimental Section). Noteworthy, the estimated values of photoconversion rate constants depend on the geometry of the measurement system and optical power. Accordingly, they are derived for our NMR setup for a relative comparison of photoisomerization processes and do not represent the absolute reaction rate constants. The details regarding the geometry of our NMR setup and the measurements are given in the Experimental Section. By these means, we determined the conversion rate constants for the bulk samples $k^{conv}_{trans\_cis} = 0.62 \times 10^{-3}\ s^{-1}$ (87% *cis* isomer at $PSS_{528\,nm}$) and $k^{conv}_{cis\_trans} = 2.63 \times 10^{-3}\ s^{-1}$ (93% *trans* isomer at $PSS_{385\,nm}$) for the *trans*→*cis* and *cis*→*trans* isomerization processes, respectively (Figures 2 and S12). Thus, the isomerization of the *cis* to the more stable *trans* form is significantly faster than the *trans*→*cis* isomerization', but still less than four times as fast' when optical power and the irradiation wavelengths are taken into account.

Perfluoroaryls have been used for S_NAr reactions with unprotected cysteine residues in synthetically and recombinantly produced peptides and proteins.[15] To probe DFAB reactivity toward unprotected cysteines, and therefore its reactivity toward peptides containing cysteines, DFAB was treated with two equivalents of *N*-Boc-cysteine in a basic environment at room temperature (Figure 1A). The formation of the resulting 4,4'-$(Cys)_2$octafluorobenzene (2Cys-OFAB) compound was confirmed by ^1H and ^{19}F NMR, purity was confirmed by HPLC (Figures S2, S3 and S4B, D). ^{19}F NMR showed two major multiplet signals at −132.9 and −149.2 ppm, corresponding to the fluorine atoms at *ortho* and *meta* positions of the *trans* isomer. The electron-donating sulfide groups induced a bathochromic shift of the π–π* band versus DFAB and a reduced splitting (1450 cm^{-1} (30 nm)) of two n–π* bands opposing the inductive effect of fluorine substitutions (Figure 1D, E). In these molecules, *cis*→*trans* isomerization was observed at 450 nm and *trans*→*cis* isomerization at 590 nm (Figure S5B). Two major signals were found in ^{19}F NMR spectrum at −130.4 and −147.0 ppm, which were assigned to the two corresponding fluorine atoms in the *cis* form after irradiation at 590 nm (Figure S3).

Design and synthesis of helical peptides

The known amphiphilic cell-penetrating α-helical peptide LK_1 was selected for modification with the perfluoroaromatic photoswitch (Figure 3A).[10,12a,16]

After successful synthesis of the peptide LK_1 by Fmoc-based solid-phase peptide synthesis (SPPS), LK_{7-11} was synthesized as a prerequisite for perfluoroaromatic stapling. Therefore, two cysteine residues were introduced in the LK_1 peptide at *i* (7) and *i*+4 (11) (LK_{7-11}) instead of lysine to maintain the hydrophobic interface of the amphiphilic helix. The formation of both peptides was confirmed by LC–MS (Figure S6A, B). These entities were isolated in high purity (over 95%; Figure 3B). Two negative bands at ~222 and ~208 nm and a positive band at ~190 nm in the circular dichroism (CD) spectra confirmed a

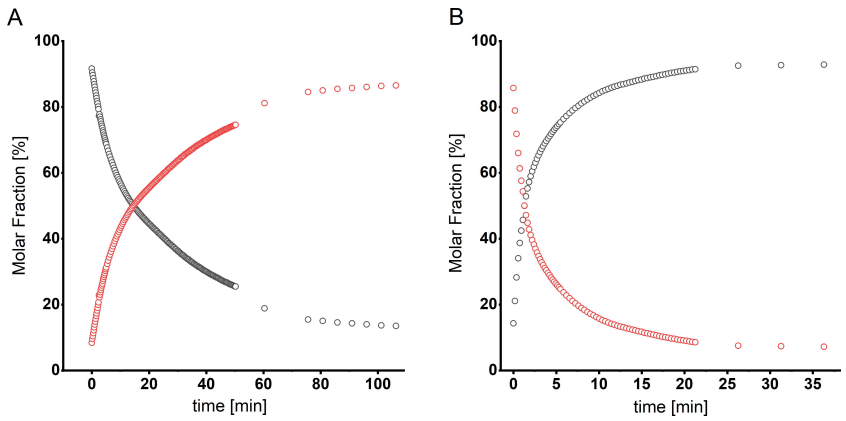

Figure 2. A) *Trans* (black) to *cis* (red) isomerization under green light irradiation (528 nm) and B) *cis* (red) to *trans* (black) isomerization of DFAB under UV light irradiation (385 nm) measured by using an *in-situ*-illumination NMR setup (^{19}F, 565 MHz, 298 K, [D_3]acetonitrile).

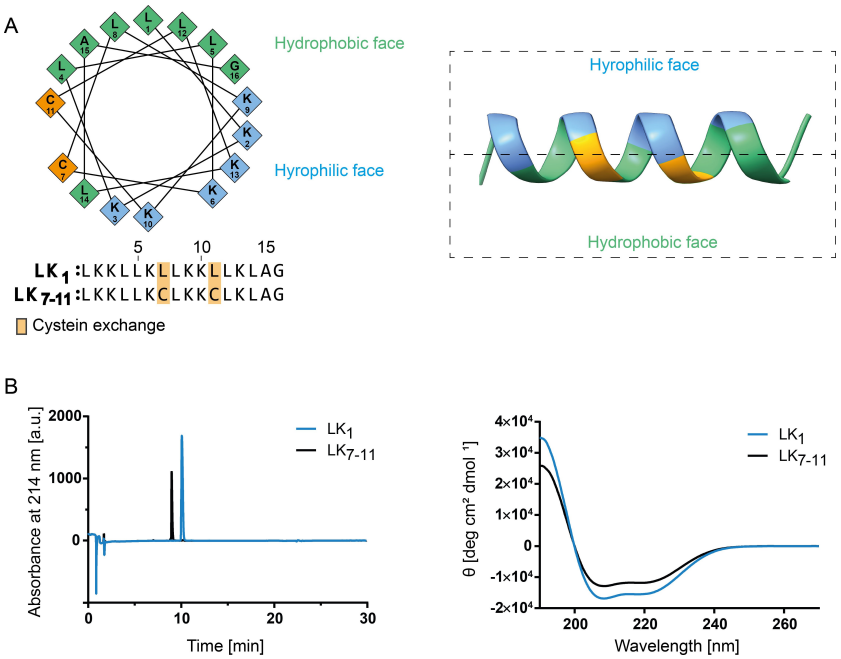

Figure 3. A) Wheel diagram and conceptual scheme of the α-helical structure of the LK peptide; green: hydrophobic, blue: hydrophilic, yellow: cysteine. Adapted with changes from refs. [12a, 16]. B) RP-HPLC analysis of LK_1 (blue) and LK_{7-11} (black). C) CD spectra of LK_1 (blue) and LK_{7-11} (black).

helical structure (Figure 3C). Therefore, the exchange of the lysines by cysteines did not change the peptides' secondary structures. LK_1 showed an ellipticity of 50.3% and LK_{7-11} an ellipticity of 38.5% in 50 mM phosphate buffer (pH 7.4) with trifluoroethanol (TFE; 50% *v/v*), respectively (Table S2).

Stapling of the LK_{7-11} peptide with DFAB and performance

As the length of 5.4 Å for the consecutive α-helix turn in the peptide LK_{7-11} and thus the distance between the cysteine residues at position *i* and *i*+4 within the peptide backbone corresponds the 4,4' carbons' end-to-end distance of an AB core in *cis* form, DFAB was exposed to 530 nm (green light) for 15 minutes before the stapling reaction (Figure 4A).[2] The peptide stapling reaction was conducted in TFE and ACN with DIPEA as a mild base for cysteine arylation.[17] Successful stapling was confirmed by LC–MS and *trans*→*cis* isomerization at 590 nm (15 min) and *cis*→*trans* isomerization at 450 nm (15 min) was analyzed by RP-HPLC (Figures 4B and S6C).

The stapled $LKST_{7-11}$ peptide exhibited differences in physical properties between the *trans*/*cis* isomeric mixtures at the two photostationary states (PSS)s, which were separated by RP-HPLC (Figure 4B). The first isomer, eluting at 8.7 min, was the *trans* isomer, in which the local distortion of the alpha helix makes the peptides more hydrophilic. The more hydrophobic *cis* isomer of the stapled peptide eluted at 10.2 min.

Longer irradiation up to 20 minutes with light at 590 nm further decreased the π–π* band electronic transition intensity, indicating that more *cis* isomer was generated. In order to define the optical properties of the stapled peptide $LKST_{7-11}$, its response was tested between 365 nm and 590 nm for 15 min (Figure S7). In terms of irradiation time and the highest content reachable for each isomer, we chose two wavelengths for the bidirectional isomerization to identify the time needed for efficient conformational change. The *cis*→*trans* isomerization at 450 nm reached the PSS_{450} in 5 minutes with a maximal *trans* content of 86% in our measurement setup (mirrored box, see details in the Experimental Section). *Trans*→*cis* isomerization at 590 nm was slower with an overall *cis* content of 89% after 22 minutes (Figures 4C and S8, Table S1). As it is known, that light in the red spectral ranges can penetrate tissue better than UV light, we also tested the response of $LKST_{7-11}$ to light with a dominant wavelength of 617 nm (Figure S11).[4m] To exclude the possibility that the isomerization is due to the spectral power distribution of the lamp at wavelengths below 600 nm, a 600 nm long-pass filter was used. Compared to isomerization at 590 nm, a significantly slower isomerization at 617 nm was observed. Despite this promising bathochromic shift, further modifications of these molecules are necessary to enable isomerization in the NIR range and thus biological application.[18]

Next, we investigated reversible switching stability of the perfluorinated photoswitch. The bidirectional switching $trans_{450\ nm} \leftrightarrow cis_{590\ nm}$ was performed for 10 cycles (Figure 4D).

Phenyl substituents stabilize the *cis* isomer and affect the spontaneous thermal relaxation to the *trans*-enriched PSS.[4b,8b] Short-lived *cis* azobenzene derivatives might be instrumental to steer fast biochemical processes, for example, ionic pumps. However, they are ineffective for longer lasting action, in which continuous exposure to light is challenging. For this reason, the spontaneous reversion from *cis*- to the more thermodynamically

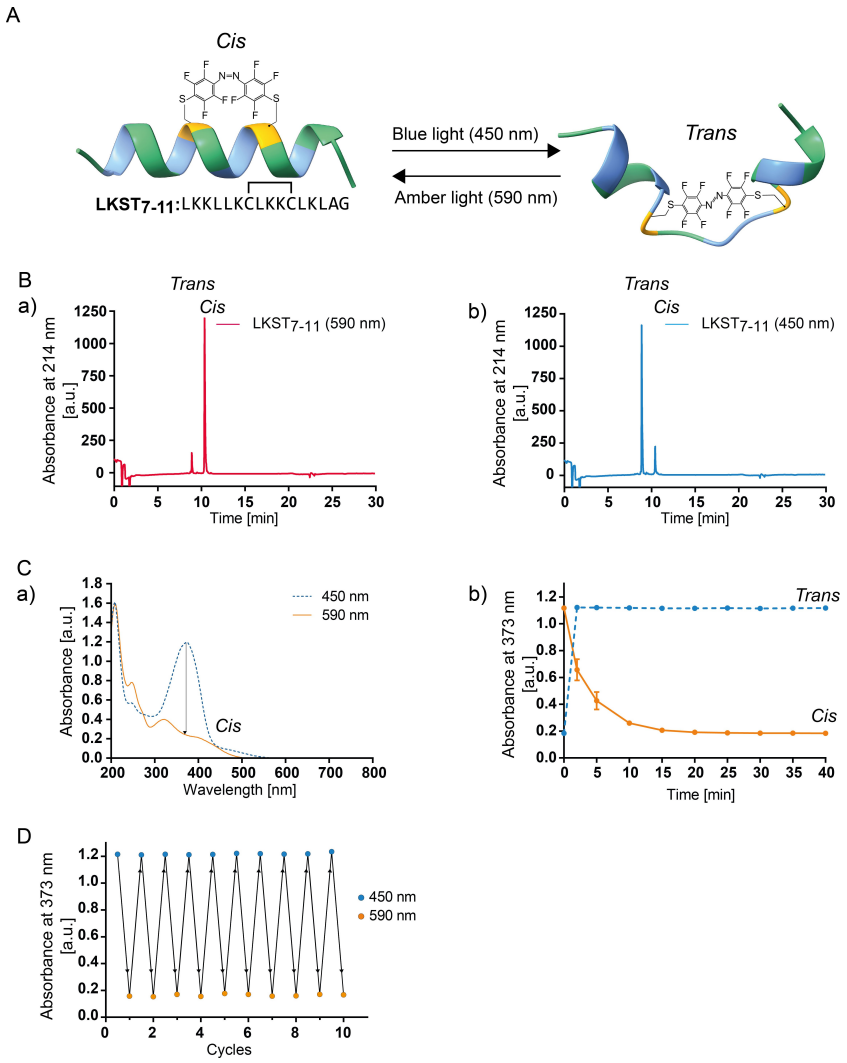

Figure 4. A) Scheme of the α-helical transition after irradiation. B) RP-HPLC analysis of $LKST_{7-11}$ irradiated at a) 590 nm and b) 450 nm for 15 min. C) a) Optical properties of $LKST_{7-11}$ after irradiation at 450 and 590 nm for 15 min with maximal difference in absorbance between the *trans* and *cis* isomer at $\lambda_{max} = 373$ nm. b) $LKST_{7-11}$ absorbance at 373 nm over 40 min under 450 and 590 nm irradiation. D) Reversible switching of the perfluorinated photoswitch evaluated by inducing bidirectional isomerization for 10 cycles at 450–590 nm light (450 nm: 5 min irradiation, 590 nm: 22 min irradiation).

stable *trans* state of $LKST_{7-11}$ was carried out both in water/ACN (50% *v/v*; Figure 5A) and pure water (Figure 5B), keeping the stapled peptide in the dark. As expected, the fluorine atoms in DFAB stabilizes the *cis*-enriched PSS of $LKST_{7-11}$ and consequently, its half-life. The *cis* isomer of the stapled peptide had a $t_{1/2}$ of 21 days in water/ACN (50% *v/v*) (Figure S9). For pure water, on the other hand, no half-life could be determined, since band broadening can be observed in the UV/Vis spectra as well as an increase in absorption over time in the region between 420 nm and beyond 500 nm, presumably due to the formation of aggregates (Figure 5). However, based on the UV/Vis spectrum, it can be assumed that the half-life in water is significantly shorter than in ACN, but longer than 4 days, enabling promising stabilization of the alpha helix in water (Figure 5).[4t,8c,19]

Next, we exposed the stapled peptide to 590 nm light irradiation for 22 minutes and studied the secondary structure by circular dichroism (Figure 6A) to verify whether this period of exposure by the two wavelengths leads to a significant difference in the helical content. The peptide in the *trans*-enriched PSS had about 13% helical content (based on the decrease in intensity of the band at $\lambda_{max} = 222$ nm). The band at $\lambda_{max} = 208$ nm slightly shifted to a shorter wavelength ($\lambda_{max} = 206$ nm) indicating a random coil peptide conformation. Exposure to 590 nm resulted in 32% helical content.

The bidirectional switching $trans_{450\,nm} \leftrightarrow cis_{590\,nm}$ was performed for three cycles (Figure 6B). The reduced end-to-end distance within the fluorinated linker of the peptide in the *cis*-enriched PSS facilitated the α-helix arrangement of the stapled peptide (Table S2).

Cytotoxicity of the stapled helical peptide was analyzed in immortalized human cervical cancer (HeLa) and murine embryotic fibroblast (NIH 3T3) cells (Figure S10). The results indicated a half maximal inhibitory concentration (IC_{50}) being lower for

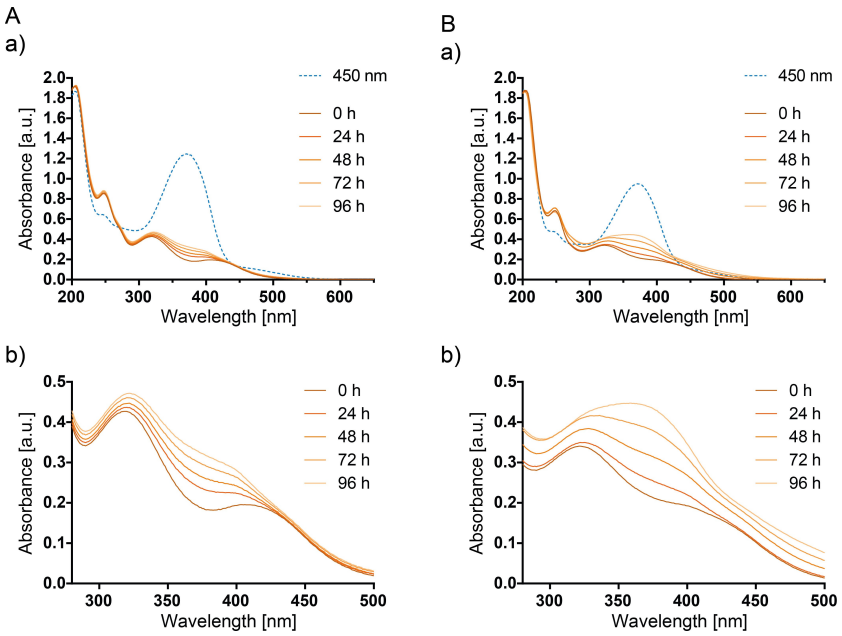

Figure 5. UV/Vis spectra of $LKST_{7-11}$ (150 μM) A) in ACN/water (50% *v/v*) and B) in water in the dark and after irradiation of the sample with $\lambda = 590$ nm for 22 min. Spectra were collected every 30 min over 4 days. For clarity, only the data after 0, 24, 48, 72 and 96 h are shown. The lower (b) spectra are magnifications.

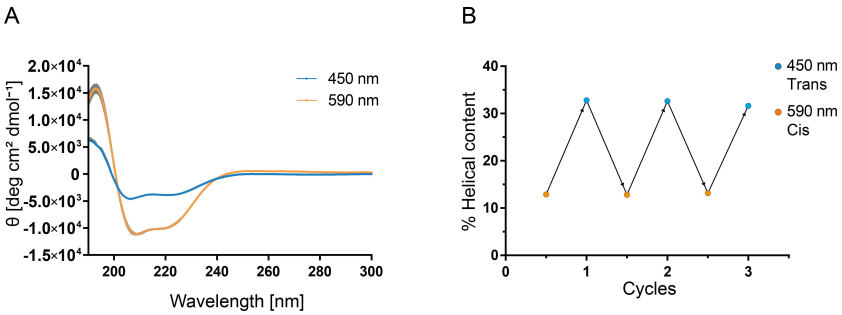

Figure 6. A) CD analysis and change of secondary structure of the stapled $LKST_{7-11}$ peptide after irradiation with 590 nm for 22 min. B) Photoswitching as analyzed by helical content of stapled $LKST_{7-11}$ peptide by inducing bidirectional isomerization for 3 cycles at 450–590 nm light (450 nm: 5 min irradiation, 590 nm: 22 min irradiation).

HeLa cells, with *trans*-$IC_{50} = 2.6$ μM (95% confidence interval (CI): 2.32 to 2.95 μM) and *cis*-$IC_{50} = 2.7$ μM (95% CI: 2.44 to 3.08 μM), and being higher for NIH 3T3 cells with *trans*-$IC_{50} = 8.9$ μM (95% CI: 7.41 to 10.68 μM) and mostly *cis*-$IC_{50} = 9.6$ μM (95% CI: 7.79 to 11.73 μM). The conformational state did not impact the cytotoxicity of the photoswitch. Even though cytotoxicity experiments are only one aspect of assessing general safety challenges, these data sets are encouraging -photoswitching can control CPPs secondary structure and therefore its properties without changing its toxicological profile.

Perspective

The principle shown here represents a promising approach to the control of secondary structures due to the simple coupling of DFAB to cysteines and the wavelengths required for isomerization. We expanded this principle to be able to control the activity of drugs. Therefore, pilot experiments were conducted with one helix of interleukin-4 (IL-4), a cytokine controlling macrophage polarization to anti-inflammatory states (desired) and B-cell maturation with a potential risk of sensitizing for atopic reactions (undesired).[20] One potential application could be an initially inactive IL-4 (to prevent B cell maturation and responses) which in response to light isomerizes into its active form (to unfold IL-4 activity at inflammatory sites). For this purpose, we synthesized the parts of the A-helix of IL-4 and

stapled it to DFAB. The secondary structure of the resulting IL-4 fragment responded to light (Figures S13 and S14).

Conclusions

Although the (relatively young) field of photocontrolling isomerization has had fascinating successes, clinical translation is still pending.[12b] This reflects the central challenge of many of these molecules responding to light at wavelengths that are also effectively absorbed by tissue, such as UV light. Consequently, insufficient intensities reach the photoswitches and prevent their performance. This drives the need for photoswitches that respond to light of longer wavelengths.[10,12b] Therefore, we developed stapled peptides that respond to amber light with *cis*↔*trans* isomerization and changes in secondary structure. Future studies should aim at shifting the absorption wavelengths of photoswitches into the NIR range to further expand their *in-vivo* applications, including use in deeper tissue layers.[18]

Experimental Section

Materials: The following chemicals were purchased from Sigma-Aldrich: *N*,*N*-diisopropylcarbodiimide (DIC), ethyl cyanohydroxyiminoacetate (Oxyma), hydroxybenzotriazole (HOBt), trifluoroacetic acid (TFA), triisopropylsilane (TIS), *N*-(*tert*-butoxycarbonyl)-L-cysteine methyl ester, 2,2′-(ethylenedioxy)diethanethiol (DODT), acetic anhydride, Fmoc-protected (L)-amino acids, RPIM 1640 medium-high glucose, fetal calf serum (FCS), penicillin-streptomycin, 2,3,4,5,6-pentafluoroaniline, 1,5-diazabiciclo(5.4.0)undec-7-ene (1,8-diazabicyclo[5.4.0]undec-7-ene) (DBU), *N*-chlorosuccinimide (NCS), tetrabutylammonium hydrogen sulfate, potassium *tert*-butoxide, dithiothreitol (DTT), trifluoroethanol (TFE), trisodium phosphate (Na_3PO_4), Rink Amide MBHA resins, cell proliferation reagent WST-1 and HPLC-grade acetonitrile (ACN). *N*,*N*-Diisopropylethylamine (DIPEA) was purchased from Carl Roth (Karlsruhe, Germany). The lamps were assembled in our laboratory and the LED modules, with different wavelength of irradiation, were purchase from LED-TECH optoelectronics GmbH (Moers, Germany). Deionized water was obtained from our in-house Merck Millipore water purification system. All other chemicals used were at least of pharmaceutical grade.

Synthesis of decafluoroazobenzene (DFAB): Pentafluoroaniline (3 g, 16.4 mmol) was dissolved in DCM (100 mL), DBU (2 equiv., 4.9 mL, 32.8 mmol) was added and the solution was stirred for 5 min. Afterwards the reaction mixture was cooled down to −78 °C in a dry ice/acetone bath and NCS (2 equiv., 4.4 g, 32.8 mmol) was added. After 30 min, the reaction was quenched with saturated sodium hydrogen carbonate solution and the dry ice/acetone bath was removed. The aqueous phase was separated, the organic phase was washed sequentially with water (300 mL) and 1 N HCl (300 mL), dried over anhydrous magnesium sulfate and the solvent was removed under reduced pressure. The crude compound was purified by column chromatography (silica, cyclohexane/DCM 9:1).[21] This afforded light orange crystals of DFAB (2.4 g, 40%). ^{19}F NMR (377 MHz, $CDCl_3$): $\delta = -146.5$ to 146.6 (o/m, 4F, *cis* isomer), −148.1 to −148.3 (o/m, 4F, *trans* isomer), −148.4 (tt, $^3J_{F-F}$, $^4J_{F-F}$ = 31.4, 3.8 Hz, 2F-*para*, *trans* isomer), −150.4 (tt, $^3J_{F-F}$, $^4J_{F-F}$ = 21.0, 1.7 Hz, 2F-*para*, *cis* isomer), −158.4 to −158.6 (o/m, 4F, *cis* isomer), −161.0 to −161.3 ppm (o/m, 4F, *trans* isomer).

Synthesis of 2Cys-OFAB: DFAB (250 mg, 0.69 mmol) and Na_3PO_4 (215 mg, 1.59 mmol, 2.3 equiv.) were dissolved in 40 mL ACN under argon. *N*-(*tert*-Butoxycarbonyl)-L-cysteine methyl ester (1.42 mmol, 284 μL, 2 equiv.) was added at once and the reaction mixture was stirred at room temperature. The reaction progress was monitored by TLC. After 1 h, the mixture was filtered through a celite pad, and the crude product was purified by column chromatography (silica, EtOAc) to afford 2Cys-OFAB (107 mg, 20%) as orange crystals. ^{1}H NMR (400 MHz, $CDCl_3$): $\delta = 5.35$ (d, $J = 6.6$ Hz, 2H, N**H**Boc) 4.61 (s, 2H, −C**H**), 3.75 (s, 6H, −C**H**$_3$), 3.63 (dd, $J = 3.9$, 14.1 Hz, 2H, −C**H**$_2$), 3.39 (dd, $J = 5.0$, 14.3 Hz, 2H, −C**H**$_2$) 1.38 (s, 18H, −COOC(C**H**$_3$)$_3$) ppm. ^{19}F NMR (377 MHz, $CDCl_3$): $\delta = -132.9$ (m, 4F-*ortho*), −149.2 (m, 4F-*meta*) ppm.

NMR analysis: NMR measurements were performed with an Avance III 400 MHz spectrometer (Karlsruhe, Germany) and the data were processed with TopSpin 4.0.7 software (Bruker, Germany). The residual solvent signals were used for spectra calibration. The coupling constants *J* are given in Hz and the chemical shifts in ppm. Multiplets were specified as s (singlet), m (multiplet), dd (doublet of doublets) and d (doublet) tt (triplet of triplets).

Peptide synthesis: Peptides LK_1 (Ac-Leu-Lys-Lys-Leu-Leu-Lys-Leu-Leu-Lys-Lys-Leu-Leu-Lys-Leu-Ala-Gly-NH_2) and LK_{7-11} (Ac-Leu-Lys-Lys-Leu-Leu-Lys-Cys-Leu-Lys-Lys-Cys-Leu-Lys-Leu-Ala-Gly-NH_2) were synthesized following a Fmoc-based solid-phase peptide synthesis protocol with Rink Amide MBHA resins. Every amino acid was coupled using DIC/Oxyma in DMF at 90 °C, while Fmoc-deprotection was performed with 20% piperidine in DMF. N-Acetylation was performed manually with 75 μL of acetic anhydride and 135 μL DIPEA in 2 mL of DMF for 30 min at room temperature. After sequential washing with DMF, DCM and diethyl ether, the peptides where fully deprotected and cleaved from the resin, by resuspending in 8 mL of TFA/DODT/TIS/H_2O (92.5:2.5:2.5:2.5) for 3 h. The peptides were precipitated from the cleavage solution with diethyl ether and centrifuged three times, in which the supernatant was discarded and replaced with cold diethyl ether. The pellet was dried under air flow.

Purification of peptides: Peptides were purified on an Äkta pure FPLC system (Marlborough, MA, USA) with a Luna 10u C18 100A (250 mm × 21.2 mm) reversed-phase column (Phenomenex Inc., Torrance, CA, USA) using a linear gradient of ACN and water with 0.1% TFA (*v*/*v*). UV-absorbance was monitored at $\lambda = 214$ nm for the unstapled peptides and at $\lambda = 214$ and 360 nm for the stapled peptide. The collected fractions were analyzed by LC–MS and HPLC. ACN and TFA were evaporated under nitrogen flow, and samples were freeze-dried in a freeze dryer Alpha 1–4 (Martin Christ Gefriertrocknungsanlagen GmbH, Osterode, Germany). The lyophilized peptides were stored at −80 °C until use.

Peptide stapling with DFAB: Solutions of 4 mM of LK_{7-11} peptide in TFE and 4 mM of DFAB in ACN were initially prepared separately. The DFAB solution was irradiated for 15 min with $\lambda = 530$ nm and subsequently combined with the peptide solution resulting in a final concentration of 2 mM. After the addition of 40 μM of DIPEA, the reaction mixture was stirred in the dark overnight. The solvent was evaporated under reduced pressure at 35 °C. The crude product was suspended in water and ACN 40% (*v*/*v*), containing 0,1% TFA (*v*/*v*) and irradiated again with $\lambda = 450$ nm for 15 min for the further purification.[17]

Liquid chromatography-mass spectrometry: The stapled and unstapled peptides were verified by using a Single Quadrupole system, consisting of an LC20AB liquid chromatograph, an SPD-20 A UV/VIS detector and an LC–MS 2020 (Shimadzu Scientific Instruments). To separate samples by LC, a Synergi 4 μm fusion-RP column (4.6 × 150 mm; Phenomenex Inc., Torrance, CA) was used

with eluent A 0.1% (*v/v*) formic acid in water and eluent B 0.1% (*v/v*) formic acid in methanol. The detection range was set from 500 to 2000 *m/z*.

Highperformance liquid chromatography analysis: The purity of the peptides was analyzed by using an Agilent HPLC system (Agilent, Santa Clara, CA, USA) consisting of a flexible pump (G7104C), a vial sampler (G7129C), a multicolumn thermostat (G7166A) with a Quick-connect heat exchanger (G7116-60051), and a VWD detector (G7114A). Separation was performed on a Zorbax 300SB CN column (150×4.6 mm), coupled with a Security guard column (Phenomenex®) at 22 °C with an ACN gradient increasing from 20 to 100% ACN in water with 0.1% TFA over 30 min at a flow rate of 1.0 mL min^{-1}. Peptides were monitored at $\lambda = 214$ nm.

Irradiation time: All given irradiation times refer to the lamps used for the tests. The specification of the lamps is given in Table S3.

Photocharacterization: The optical properties and the assessment of quality of *trans*→*cis* isomerization and *vice versa* were analyzed on a UV/Vis spectrometer Genesys 10S from Thermo Scientific. Samples were filled in a QS quartz cuvette (10 mm) from Hellma Analytics (Mülheim, Germany) and the spectra were recorded between the range of 200 to 650 nm. The exposure to light at different wavelengths was performed by directly placing the cuvette in a mirrored box (22×10×14 cm) and maintaining the distance of 1 cm from the light source. DFAB and 2Cys-OFAB were dissolved in ACN at a concentration of 50 μM. The stapled peptide was dissolved in ACN/water (20:80, *v/v*), resulting in a concentration of 150 μM. Each irradiation lasted 15 min if not otherwise stated. For the measurements with 617 nm, a solution of $LKST_{7-11}$ (150 μM) was irradiated in a quartz cuvette in a darkened box. The distance between the cuvette and the lamp was 1 cm, with a long-pass filter (Edmund Optics, 600 nm, PO #4500337369-00-21057) attached between the lamp and the cuvette.

Photostability: $\lambda = 450$ and 590 nm LED lamps were selected for the reversible isomerization of stapled peptides. 150 μM of the $LKST_{7-11}$ in ACN/water (20:80, *v/v*) was irradiated, and UV-Vis spectra were collected at 2, 5, 10, 15, 20, 25, 30, 35 and 40 min. Changes in the absorbance (blue and red shift light exposure, respectively) were monitored at $\lambda = 373$ nm, corresponding to the major band intensity differences between the *trans* and *cis* form ($\max\Delta A_{trans}$-A_{cis}). In addition, photostability was analyzed by inducing bidirectional isomerization for ten cycles.

***Cis-trans* isomer quantification**: $LKST_{7-11}$ was dissolved in water/ACN 20% (*v/v*) and irradiated at different wavelengths ($\lambda = 450$ and 590 nm) for different times. Briefly, 70 μL (200 μM) was analyzed by HPLC, as indicated above. Peptide monitoring was performed at the isosbestic point at $\lambda = 272$ nm. Quantification of the *cis* content was determined by integration of the peaks detected at $t_R = 8.73$ and 10.22 min, corresponding to the *trans* and *cis* isomers, respectively.

***Cis*-isomer half-life**: The spontaneous reversion from *cis* to the more thermodynamically stable *trans* state was carried out both in water/ACN 50% (*v/v*) and pure water, keeping the stapled peptide (150 μM) in the dark. After irradiation at $\lambda = 590$ nm for 22 min, spectra were collected every 30 min over 4 days. In order to calculate the effective half-life of the *cis* isomer, the absorbance at $\lambda = 373$ nm was used. As *cis* to *trans* isomerization follows first-order kinetics, $\ln((A_0-A_\infty)/(A_t-A_\infty))$ was plotted against time. The half-life was then calculated from the equation $t_{1/2} = \ln(2)/k$.[4k]

Circular dichroism (CD) analysis of stapled peptides: Circular dichroism (CD) spectra were obtained by a Jasco J-715 Spectropolarimeter with a Jasco PS-150J Spectropolarimeter Power Supply. The samples were placed in a 1.0 mm path-length Quartz cell. CD was scanned from 190 to 300 nm with a setup of 1 s integration, 1-nm-step resolution, and 10 nm bandwidth. The results from three scans were averaged. The α-helicity was measured for LK_1 and LK_{7-11} and $LKST_{7-11}$ (150 μM). Unstapled peptides were dissolved in 50 mM phosphate buffer (PB, pH 7.4) TFE 50% (*v/v*) and 1 mM of DTT, while the stapled peptide was dissolved in PB (pH 7.4):TFE 50% (*v/v*). CD spectra were recorded after light exposure ($\lambda = 590$ and 450 nm).

α-Helical content determination: For comparisons, molar residue ellipticity (MRE) was determined by correcting spectra with peptide concentration according to Equation (1). MRW is the mean residual weight, *c* is concentration in mg mL^{-1}, *l* the path length in mm.[10]

$$\mathrm{MRE}\ (\mathrm{deg cm^2 dmol^{-1}}) = \frac{[\mathrm{mdegree}]\ \mathrm{MRW}}{c\ l} \quad (1)$$

α-Helical content was calculated referring to the MRE at 222 nm, assuming the 30000 value is found for 100% helical peptides [Eq. (2)].

$$\%\ \alpha\text{-helical content} = \frac{[\theta]_{222}}{30000} \times 100 \quad (2)$$

Cytotoxicity: Cytotoxicity was tested in HeLa (human cervical cancer) and NIH 3T3 (murine embryotic fibroblast cells) cells, respectively. Cells were maintained in RPMI 1640 (HeLa) and DMEM (NIH 3T3) culture media containing 10% FBS and 1% P/S. Cells were seeded in a 96-well plate (HeLa 5000 cells/100 μL/well, NIH 3T3 3000 cells/100 μL/well) and incubated at 37 °C and 5% CO_2 for 24 h. To determine the cytotoxicity of $LKST_{7-11}$, a stock solution (250 μM) was prepared and sterile filtered (0.22 μm PES filter media) prior to use. The stock solution was irradiated at $\lambda = 450$ nm for 10 min or at $\lambda = 590$ nm for 30 min, respectively. Both peptides were diluted from 125 μM to 0.48 nM and added to the cells. Cells were incubated for 24 h at 37 °C and 5% CO_2. After incubation, 10 μL WST-1 reagent were added to each well and cells were incubated for 4 h at 37 °C according to manufacturer instructions. Every 30 min, cells were analyzed, and the absorbance of the soluble formazan product at 450 nm as well as background noise at 630 nm were determined using an Infinite 200Pro (Tecan, Männerdorf, Switzerland).

Setup for *in-situ* illumination NMR spectroscopy: The setup for *in-situ* illumination NMR spectroscopy, including the electronic setup with LED power device, the optical fiber, the NMR tube with the screw connectors, was built according to the setup published by Gschwind and co-workers with some modifications.[14,22] NMR spectra were recorded on an Avance Neo I 600 from Bruker. A PI HR-TBP600S3-BBF/H/11B/D-5.0-Z DP probe was used for the measurements of ^{19}F NMR spectra using the Topspin 4.14 software version.

Electronic setup: A real-time clock pulse (RCP) adapter box (RCPBOX, Bruker) was connected with a RJ45 cable to the Avance Neo I console providing 4 input and 4 output ports for the TTL signals with a resolution of 80 MHz. A BNC cable connected one TTL output with the LED power device. The following high power LEDs were used for illumination: 385 nm, Luminus SST-10 UV, powered with 4 V, 1500 mA, 46 mW at the sample; 528 nm, OSRAM Oslon SSL 80, powered with 3.5 V, 1000 mA, 25 mW at the sample. The optical power at the sample was measured with an 843-R power meter equipped with an 818-UV/DB detector (200–1100 nm; Newport) by bringing a LED-coupled fiber (Thorlabs, 4.5 m, original with cladding), surrounded by the glass insert, perpendicularly in direct contact with the round-shaped detector.

Spectroscopy setup: an optical fiber with 1000 µm core diameter and 5.7 m length (Thorlabs, Custom Patch Cable-Fiber: FP1000URT, Tubing: FT038, SMA to flat cleave large core) was used to guide the LED light into the NMR tube. Jacketing and outer cladding were removed by using a stripping tool (Thorlabs, M44S63 Fiber Stripping Tool) to make the fiber fit into the glass insert of the NMR tube. In the receiver coil area, the fiber was roughened with the help of a diamond needle file (Heson S2012/D30) at a length of 38 mm allowing radial illumination. The fiber end was in contact with the glass insert, which touched the bottom of the NMR tube.

The LED housing consists of a cubic box with detachable walls and cover, providing space for three LED-heat sink combinations. Each LED board covered with heat-conducting paste (Fischer-Elektronik-Wärmeleitpaste, LT-3251) was screwed on a metal disk, which was then screwed together with commercially available heat sinks. The respective heat sink-LED combination was mounted on a height-adjustable post holder (Thorlabs, TR40/M and PH40/M). Coupling the LED and fiber was carried out by placing the LED as near as possible in front of a fiber connector adapter (Thorlabs, SM1MA, CP33/M) with the help of assembly rods (Thorlabs, ER2-P4). Silicone lenses were cut off from the LEDs.

During the actual experiment, the fiber protected by a coaxial glass insert (NI5CCI-B-QTZ, Eurisotop) was inserted into a 600 MHz amberized 17.8 cm (7″) NMR tube (S-5-600-AT-7, Eurisotop). A customized screw cap, a union nut, and O-rings (Ludwig Meister 270-OR 4.00X 1.00 and 270-OR 5.00X 1.00) allowed an airtight connection of the NMR tube and coaxial insert. In a similar fashion, a plastic tube with a second screw connection was manufactured in order to stabilize the fiber and tightly connect it with the coaxial insert.

Investigation of the photoisomerization processes in the optical fiber-based NMR illumination setup: A degassed solution of DFAB in [D_3]acetonitrile (0.08 M, 0.2 mL) was irradiated by using the above-described setup. To this end, a pulse sequence was written which allowed for the illumination within a defined period of time. At the end of this period the LED was turned off and a standard pulse sequence for the acquisition of a quantitative ^{19}F NMR spectrum with 8 scans and a relaxation time of 3 s followed. The LED was then turned back on and the cycle was iterated a given number of times. First, the DFAB sample was irradiated with 385 nm UV light for 15 min until the photostationary state (PSS) was reached. Then the sample was irradiated with 528 nm green light for short time intervals to determine the *trans*→*cis* bulk photoconversion rate constant in the given setup. After reaching the equilibrium the sample was again irradiated with 385 nm light for short time intervals to determine the *cis*→*trans* bulk photoconversion rate constant in the given setup. The photoinduced isomerization process can be illustrated as follows:

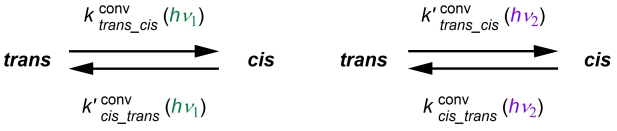

At a given wavelength $h\nu_1$ and light intensity I, the *trans* isomer is converted to the *cis* with a given conversion rate constant $k^{conv}_{trans\_cis}$. The same wavelength also enables the reverse reaction with rate constant $k'^{conv}_{cis\_trans}$. The same applies to the *cis* to *trans* isomerization. Azobenzene photoswitches usually undergo a thermal *cis* to *trans* isomerization but since perfluorinated azobenzenes show high thermal stabilities, this influence will be neglected in this derivation of rate constants.[8c] Therefore, a pseudo first order reversible reaction kinetics is assumed for the above illustrated process, as described mathematically in the literature.[23] [Eq. (3)]

$$\begin{aligned}\frac{d[trans]}{dt} &= -k^{conv}_{trans\_cis}[trans] + k'^{conv}_{cis\_trans}[cis] = -k^{conv}_{trans\_cis}[trans] \\ &+k'^{conv}_{cis\_trans}([trans]_0 + [cis]_0 - [trans]) \\ &= -\left(k^{conv}_{trans_{cis}} + k'^{conv}_{cis_{trans}}\right)[trans] + k'^{conv}_{cis_{trans}} \cdot c_{tot}\end{aligned} \quad (3)$$

[*trans*] represents the concentration of *trans* isomer at a given time t and c_{tot} the total concentration of DFAB sample. As DFAB in PSS always exists as a mixture of *trans* and *cis* isomers, the initial concentrations $[trans]_0$ and $[cis]_0$ do not equal zero.

With the expression for the equilibrium constant (for a given wavelength and light intensity) at the PSS [Eq. (4)]

$$K^{conv}_{trans\_cis} = \frac{k^{conv}_{trans\_cis}}{k'^{conv}_{cis\_trans}} = \frac{[cis]_{eq}}{[trans]_{eq}} \quad (4)$$

and the expression for the equilibrium concentration $[trans]_{eq}$ [Eq. (5)]

$$[trans]_{eq} = \frac{k'^{conv}_{cis\_trans} \cdot c_{tot}}{k^{conv}_{trans\_cis} + k'^{conv}_{cis\_trans}} \quad (5)$$

Equation (1) may be expressed as Equation (6):

$$\ln\left(\frac{[trans] - [trans]_{eq}}{[trans]_0 - [trans]_{eq}}\right) = -\left(k^{conv}_{trans_{cis}} + k'^{conv}_{cis_{trans}}\right) \cdot t \quad (6)$$

By plotting $\ln\left(\frac{[trans]-[trans]_{eq}}{[trans]_0-[trans]_{eq}}\right)$ against t, a linear regression with slope m equal to $-(k_{trans\ cis} + k'_{cis\ trans})$ can be obtained. Subsequently, $k^{conv}_{trans\_cis}$ and $k'^{conv}_{cis\_trans}$ can be calculated from Equation (4) as follows [Eqs (7) and (8)]:

$$k^{conv}_{trans\_cis} = -\frac{m}{1 + \frac{[trans]_{eq}}{[cis]_{eq}}} \quad (7)$$

$$k'^{conv}_{cis\_trans} = -\frac{m}{1 + \frac{[cis]_{eq}}{[trans]_{eq}}} \quad (8)$$

By analogy, the values for $k^{conv}_{cis\_trans}$ and $k'^{conv}_{trans\_cis}$ for the *cis* to *trans* isomerization can be derived.

Acknowledgements

We gratefully acknowledge financial support from Bayerische Forschungsstiftung (AZ-1204-16) for E.C. and from the Deutsche Forschungsgemeinschaft (DFG #ME 3820/7-1) for L.M.. H.G. acknowledges the support by the International Doctoral Program "Receptor Dynamics: Emerging Paradigms for Novel Drugs" funded within the framework of the Elite Network of Bavaria (ENB). Financial support by the German Research Foundation (DFG) for M.D. under DFG DE1546/10-1 is acknowledged. A.N.-K. thanks the German Research Foundation (DFG) for the Emmy-Noether fellowship (NO 1459/1-1) and the Hector Fellow Academy for financial support. A. N.-K., R. B. and P. T. G. would like to express their gratitude to Prof. Ruth M. Gschwind and Willibald Stockerl (University of Regensburg) for helpful discussions regarding the setup for combined in situ illumination NMR-UV/Vis Spectroscopy.

P.T.G. would also like to thank Laura Wolz from the NMR department (University of Würzburg) for technical support and her contribution to carrying out the NMR experiments. M.R. would like to thank Prof. Thomas Müller for cysteine exchange in the IL-4 motif. Open Access funding enabled and organized by Projekt DEAL.

Conflict of Interest

The authors declare no conflict of interest.

Data Availability Statement

The data that support the findings of this study are available from the corresponding author upon reasonable request.

Keywords: amber light · decafluoroazobezene · peptide stapling · photocontrol · perfluoroarylation

[1] a) K. Hüll, J. Morstein, D. Trauner, *Chem. Rev.* **2018**, *118*, 10710–10747; b) M. Scheiner, A. Sink, M. Hoffmann, C. Vrigneau, E. Endres, A. Carles, C. Sotriffer, T. Maurice, M. Decker, *J. Am. Chem. Soc.* **2022**, *144*, 3279–3284; c) D. A. Rodríguez-Soacha, J. Fender, Y. A. Ramírez, J. A. Collado, E. Muñoz, R. Maitra, C. Sotriffer, K. Lorenz, M. Decker, *ACS Chem. Neurosci.* **2021**, *12*, 1632–1647.

[2] a) C. Dugave, L. Demange, *Chem. Rev.* **2003**, *103*, 2475–2532; b) E. Merino, M. Ribagorda, *Beilstein J. Org. Chem.* **2012**, *8*, 1071–1090.

[3] H. Rau, *Angew. Chem. Int. Ed. Engl.* **1973**, *12*, 224–235.

[4] a) R. J. Mart, R. K. Allemann, *Chem. Commun. (Camb.)* **2016**, *52*, 12262–12277; b) A. A. Beharry, G. A. Woolley, *Chem. Soc. Rev.* **2011**, *40*, 4422–4437; c) L. Guerrero, O. S. Smart, C. J. Weston, D. C. Burns, G. A. Woolley, R. K. Allemann, *Angew. Chem. Int. Ed.* **2005**, *44*, 7778–7782; *Angew. Chem.* **2005**, *117*, 7956–7960; d) H. Gerwe, F. He, E. Pottie, C. Stove, M. Decker, *Angew. Chem.* **2022**, *134*, e202203034; e) M. Volgraf, P. Gorostiza, S. Szobota, M. R. Helix, E. Y. Isacoff, D. Trauner, *J. Am. Chem. Soc.* **2007**, *129*, 260–261; f) P. Leippe, J. A. Frank, *Curr. Opin. Struct. Biol.* **2019**, *57*, 23–30; g) J. Broichhagen, M. Schönberger, S. C. Cork, J. A. Frank, P. Marchetti, M. Bugliani, A. M. J. Shapiro, S. Trapp, G. A. Rutter, D. J. Hodson, D. Trauner, *Nat. Commun.* **2014**, *5*, 5116; h) N. Chander, J. Morstein, J. S. Bolten, A. Shemet, P. R. Cullis, D. Trauner, D. Witzigmann, *Small* **2021**, *17*, 2008198; i) S. R. Deka, S. Yadav, M. Mahato, A. K. Sharma, *Colloids Surf. B* **2015**, *135*, 150–157; j) X. Chi, X. Ji, D. Xia, F. Huang, *J. Am. Chem. Soc.* **2015**, *137*, 1440–1443; k) J. Wiest, J. Kehrein, M. Saedtler, K. Schilling, E. Cataldi, C. A. Sotriffer, U. Holzgrabe, T. Rasmussen, B. Bottcher, M. Cronin-Golomb, M. Lehmann, N. Jung, M. Windbergs, L. Meinel, *Mol. Pharm.* **2020**, *17*, 4704–4708; l) M. L. Rahman, T. K. Biswas, S. M. Sarkar, M. M. Yusoff, A. R. Yuvaraj, S. Kumar, *J. Colloid Interface Sci.* **2016**, *478*, 384–393; m) C. Ash, M. Dubec, K. Donne, T. Bashford, *Lasers Med. Sci.* **2017**, *32*, 1909–1918; n) D. Martinez-Lopez, A. Babalhavaeji, D. Sampedro, G. A. Woolley, *Beilstein J. Org. Chem.* **2019**, *15*, 3000–3008; o) M. Dong, A. Babalhavaeji, C. V. Collins, K. Jarrah, O. Sadovski, Q. Dai, G. A. Woolley, *J. Am. Chem. Soc.* **2017**, *139*, 13483–13486; p) S. Samanta, A. Babalhavaeji, M. X. Dong, G. A. Woolley, *Angew. Chem. Int. Ed.* **2013**, *52*, 14127–14130; *Angew. Chem.* **2013**, *125*, 14377–14380; q) S. Samanta, A. A. Beharry, O. Sadovski, T. M. McCormick, A. Babalhavaeji, V. Tropepe, G. A. Woolley, *J. Am. Chem. Soc.* **2013**, *135*, 9777–9784; r) A. M. Ali, G. A. Woolley, *Org. Biomol. Chem.* **2013**, *11*, 5325–5331; s) T. S. Al-Deen, D. B. Hibbert, J. M. Hook, R. J. Wells, *Accredit. Qual. Assur.* **2004**, *9*, 55–63; t) D. Bleger, J. Schwarz, A. M. Brouwer, S. Hecht, *J. Am. Chem. Soc.* **2012**, *134*, 20597–20600.

[5] M. Döbbelin, A. Ciesielski, S. Haar, S. Osella, M. Bruna, A. Minoia, L. Grisanti, T. Mosciatti, F. Richard, E. A. Prasetyanto, *Nat. Commun.* **2016**, *7*, 1–10.

[6] a) Z. Zhang, D. C. Burns, J. R. Kumita, O. S. Smart, G. A. Woolley, *Bioconjugate Chem.* **2003**, *14*, 824–829; b) C. Hoppmann, I. Maslennikov, S. Choe, L. Wang, *J. Am. Chem. Soc.* **2015**, *137*, 11218–11221.

[7] a) S. Samanta, T. M. McCormick, S. K. Schmidt, D. S. Seferos, G. A. Woolley, *Chem. Commun. (Camb.)* **2013**, *49*, 10314–10316; b) M. Dong, A. Babalhavaeji, M. Hansen, L. Kalman, G. Woolley, *Chem. Commun.* **2015**, *51*, 12981–12984.

[8] a) L. Agnetta, M. Bermudez, F. Riefolo, C. Matera, E. Claro, R. Messerer, T. Littmann, G. Wolber, U. Holzgrabe, M. Decker, *J. Med. Chem.* **2019**, *62*, 3009–3020; b) X.-M. Liu, X.-Y. Jin, Z.-X. Zhang, J. Wang, F.-Q. Bai, *RSC Adv.* **2018**, *8*, 11580–11588; c) C. Knie, M. Utecht, F. Zhao, H. Kulla, S. Kovalenko, A. M. Brouwer, P. Saalfrank, S. Hecht, D. Bléger, *Chem. Eur. J.* **2014**, *20*, 16492–16501.

[9] A. L. Leistner, S. Kirchner, J. Karcher, T. Bantle, M. L. Schulte, P. Godtel, C. Fengler, Z. L. Pianowski, *Chemistry* **2021**, *27*, 8094–8099.

[10] G. C. Kim, J. H. Ahn, J. H. Oh, S. Nam, S. Hyun, J. Yu, Y. Lee, *Biomacromolecules* **2018**, *19*, 2863–2869.

[11] a) K. Desale, K. Kuche, S. Jain, *Biomater. Sci.* **2021**, *9*, 1153–1188; b) C. Berry, *Nanomedicine* **2008**, *3*, 357–365; c) D. M. Copolovici, K. Langel, E. Eriste, Ü. Langel, *ACS Nano* **2014**, *8*, 1972–1994; d) H. Derakhshankhah, S. Jafari, *Biomed. Pharmacother.* **2018**, *108*, 1090–1096; e) P. Boisguérin, S. Deshayes, M. J. Gait, L. O'Donovan, C. Godfrey, C. A. Betts, M. J. Wood, B. Lebleu, *Adv. Drug Delivery Rev.* **2015**, *87*, 52–67.

[12] a) S. Jang, S. Hyun, S. Kim, S. Lee, I.-S. Lee, M. Baba, Y. Lee, J. Yu, *Angew. Chem. Int. Ed.* **2014**, *53*, 10086–10089; *Angew. Chem.* **2014**, *126*, 10250–10253; b) G. C. Kim, D. H. Cheon, Y. Lee, *Biochim. Biophys. Acta Proteins Proteomics* **2021**, *1869*, 140604.

[13] M. Moiola, M. G. Memeo, P. Quadrelli, *Molecules* **2019**, *24*, 3654.

[14] A. Seegerer, P. Nitschke, R. M. Gschwind, *Angew. Chem. Int. Ed.* **2018**, *57*, 7493–7497; *Angew. Chem.* **2018**, *130*, 7615–7619.

[15] a) A. M. Spokoyny, Y. Zou, J. J. Ling, H. Yu, Y. S. Lin, B. L. Pentelute, *J. Am. Chem. Soc.* **2013**, *135*, 5946–5949; b) T. Luhmann, S. K. Mong, M. D. Simon, L. Meinel, B. L. Pentelute, *Org. Biomol. Chem.* **2016**, *14*, 3345–3349; c) W. D. G. Brittain, C. R. Coxon, *Chem. Eur. J.* **2021**, *27*, 10–23.

[16] a) S. Hyun, J. Na, S. J. Lee, S. Park, J. Yu, *ChemBioChem* **2010**, *11*, 767–770; b) Y. Lee, S. Hyun, H. J. Kim, J. Yu, *Angew. Chem. Int. Ed.* **2008**, *47*, 134–137; *Angew. Chem.* **2008**, *120*, 140–143.

[17] D. Gimenez, A. Dose, N. L. Robson, G. Sandford, S. L. Cobb, C. R. Coxon, *Org. Biomol. Chem.* **2017**, *15*, 4081–4085.

[18] a) A. M. Smith, M. C. Mancini, S. Nie, *Nat. Nanotechnol.* **2009**, *4*, 710–711; b) A. Alabugin, *Photochem. Photobiol.* **2019**, *95*, 722–732.

[19] M. A. Kienzler, A. Reiner, E. Trautman, S. Yoo, D. Trauner, E. Y. Isacoff, *J. Am. Chem. Soc.* **2013**, *135*, 17683–17686.

[20] a) D. Haas, N. Hauptstein, M. Dirauf, M. D. Driessen, M. Ruopp, U. S. Schubert, T. Lühmann, L. Meinel, *Bioconjugate Chem.* **2021**, *33*, 97–104; b) V. Spieler, M.-G. Ludwig, J. Dawson, B. Tigani, A. Littlewood-Evans, C. Safina, H. Ebersbach, K. Seuwen, M. Raschig, B. Ter Mors, *J. Controlled Release* **2020**, *326*, 172–180; c) O. R. Zekavat, E. Nikpendar, S. Haghpanah, N. Shokrgozar, S. J. Dehghani, N. Arandi, *BMC Pediatr.* **2022**, *22*, 1–7; d) F. Xia, C. Deng, Y. Jiang, Y. Qu, J. Deng, Z. Cai, Y. Ding, Z. Guo, J. Wang, *Autophagy* **2018**, *14*, 450–464.

[21] A. Antoine John, Q. Lin, *J. Org. Chem.* **2017**, *82*, 9873–9876.

[22] C. Feldmeier, H. Bartling, E. Riedle, R. M. Gschwind, *J. Magn. Reson.* **2013**, *232*, 39–44.

[23] J. d. P. P. W. Atkins, *Physikalische Chemie, Vol. 6*, Wiley-VCH, **2021**.

Manuscript received: September 30, 2022
Revised manuscript received: December 23, 2022
Accepted manuscript online: December 25, 2022
Version of record online: January 26, 2023